IOP Publishing Phys. Med. Biol. 65 (2020) 225018 https://doi.org/10.1088/1361-6560/abb7c1

Physics in Medicine & Biology

IPEM Institute of Physics and Engineering in Medicine

PAPER

RECEIVED
21 June 2020

REVISED
8 August 2020

ACCEPTED FOR PUBLICATION
11 September 2020

PUBLISHED
13 November 2020

Role of skin tissue layers and ultra-structure in transcutaneous electrical stimulation including tDCS

Niranjan Khadka and Marom Bikson

Department of Biomedical Engineering, The City College of New York, CUNY, New York, NY 10031, United States of America

E-mail: bikson@ccny.cuny.edu and nironzan@gmail.com

Keywords: skin, transcutaneous electrical stimulation, ultra-structure, current density edge effect, FEM

Abstract

Background. During transcranial electrical stimulation (tES), including transcranial direct current stimulation (tDCS) and transcranial alternating current stimulation (tACS), current density concentration around the electrode edges that is predicted by simplistic skin models does not match experimental observations of erythema, heating, or other adverse events. We hypothesized that enhancing models to include skin anatomical details, would alter predicted current patterns to align with experimental observations. *Method*. We develop a high-resolution multi-layer skin model (epidermis, dermis, and fat), with or without additional ultra-structures (hair follicles, sweat glands, and blood vessels). Current flow patterns across each layer and within ultra-structures were predicted using finite element methods considering a broad range of modeled tissue parameters including 78 combinations of skin layer conductivities (S m^{-1}): epidermis (standard: 1.05×10^{-5}; range: 1.05×10^{-6} to 0.465); dermis (standard: 0.23; range: 0.0023 to 23), fat (standard: 2×10^{-4}; range: 0.02 to 2×10^{-5}). The impact of each ultra-structures in isolation and combination was evaluated with varied basic geometries. An integrated final model is then developed. *Results*. Consistent with prior models, current flow through homogenous skin was annular (concentrated at the electrode edges). In multi-layer skin, reducing epidermis conductivity and/or increasing dermis conductivity decreased current near electrode edges, however no realistic tissue layer parameters produced non-annular current flow at both epidermis and dermis. Addition of just hair follicles, sweat glands, or blood vessels resulted in current peaks around each ultrastructure, irrespective of proximity to electrode edges. Addition of only sweat glands was the most effective approach in reducing overall current concentration near electrode edges. Representation of blood vessels resulted in a uniform current flow across the vascular network. Finally, we ran the first realistic model of current flow across the skin. *Conclusion*. We confirm prior models exhibiting current concentration near hair follicles or sweat glands, but also exhibit that an overall annular pattern of current flow remains for realistic tissue parameters. We model skin blood vessels for the first time and show that this robustly distributes current across the vascular network, consistent with experimental erythema patterns. Only a state-of-the-art precise model of skin current flow predicts lack of current concentration near electrode edges across all skin layers.

1. Introduction

Low-intensity transcranial electrical stimulation (tES), including transcranial direct current stimulation (tDCS) and transcranial alternating current stimulation (tACS), deliver current through electrodes positioned at the scalp (Nitsche *et al* 2008, Bikson *et al* 2016). As a result, current densities in the skin are much higher than in the targeted brain tissue (Bikson *et al* 2018). Related to this, while low-intensity tES is typically well tolerated, mild adverse events are related to skin current flow including transient cutaneous sensations (tingling, itching, sensation of burning) and erythema (Bikson *et al* 2009, Fertonani *et al* 2015,

Aparício *et al* 2016, Bikson *et al* 2016, Paneri *et al* 2016, Antal *et al* 2017, Poreisz *et al* 2007). The occurrence of these mild adverse events under (or near) electrodes is consistent with higher current density at the skin under the electrodes. Understanding and optimizing skin current flow is of interest to: (1) further enhance tES tolerability; (2) support higher (e.g. 3–4 mA) current stimulation (Khadka *et al* 2019, Reckow *et al* 2018, Workman *et al* 2020); (3) enhance blinding in trials (Kessler *et al* 2012, Wallace *et al* 2016, Ezquerro *et al* 2017, Greinacher *et al* 2018, Fonteneau *et al* 2019, Turi *et al* 2019); (4) understand extra-cranial nerve stimulation (Asamoah *et al* 2019, Adair *et al* 2020); (5) generally enhance tES technology such as reliability in remote settings (Shaw *et al* 2017), dry-electrodes (Khadka *et al* 2018a), or reducing voltage requirements (Hahn *et al* 2013).

The design of tES electrodes fundamentally impacts tES tolerability, effectiveness, and trial design (e.g. perception levels and so sham effectiveness). Approaches to optimize electrodes for tES has focused on managing electrochemical production (Minhas *et al* 2010) or skin current flow (Khadka *et al* 2018a), which are impacted by electrolyte composition and contact-area (Dundas *et al* 2007, Ambrus *et al* 2011, Minhas *et al* 2011). Because skin current flow patterns cannot be accurately measured, finite element method (FEM) current flow models are relied on for reliable prediction (Miranda *et al* 2006, Sha *et al* 2008, Minhas *et al* 2011, Kronberg and Bikson 2012). Prior models consider skin as simplistic by representing the scalp as one (homogenous; (Datta *et al* 2009b; Saturnino *et al* 2015)) or few (e.g. fat and skin; (Sha *et al* 2008, Truong *et al* 2013, Gomez-Tames *et al* 2016, Khadka *et al* 2018b)) compartments. There appears a fundamental mismatch between the distribution of current flow as predicted by these simple FEM skin current flow models and reported experimental outcomes. Models predict an extreme concentration of current density around electrode edges (Miranda *et al* 2006, Datta *et al* 2009a, Saturnino *et al* 2015, Gomez-Tames *et al* 2016), while erythema and temperature are largely uniform (Ezquerro *et al* 2017, Khadka *et al* 2018b). Lasting skin irritation is not an expected effect of low-intensity tES, but when standard and established protocols (Woods *et al* 2016) are not followed, the occurrences of skin lesions is not typically at electrode edges (Shiozawa *et al* 2013, Wang *et al* 2015).

If simplistic skin models do not accurately predict current flow distribution, the reason seems evident: they do not represent the known structure of skin (Panescu *et al* 1993). Epidermis is the outer layer of the skin including the exceptionally resistive stratum corneum (Yamamoto and Yamamoto 1976). The epidermis and underlying dermis layer are penetrated by electrically conductive sweat glands (Kolarsick *et al* 2011, Yousef *et al* 2020) and electrically resistive hair follicles. The epidermis is avascular while the dermis includes a high blood vessel density (Kolarsick *et al* 2011, Luna *et al* 2015, Yousef *et al* 2020). The remaining tissue layer of the skin is subcutaneous including fat and muscles (Kolarsick *et al* 2011, Yousef *et al* 2020). Few FEM studies considered the role of skin structure in current flow. We previously developed a multi-layer skin model to predict skin heating during tDCS (Khadka *et al* 2018b). Sha and colleagues developed a 2D FEM model of multi-layer skin with a single geometric sweat duct which concentrated current density (Sha *et al* 2008). Gomez-Tames and colleagues developed a three-layer skin model with geometric hair follicles and sweat glands which reduced current concentration at the edges due to current dispersion via sweat glands.

Experiments characterizing the complex skin impedance often accompanied the development of lumped-parameter models. Spanning decades, both experiments and simulations were largely 1D, considering variation in depth but not across the skin (Tregear 1966, Lykken 1970). These studies confirmed that current concentrates in discrete channels (e.g. sweat ducts) (Mueller *et al* 1953, Geldard 1974). They also demonstrated dependence on environmental factors (e.g. sweat) (Suchi 1955, Pierard-Franchimont and Pierard 2015) including saturation by the electrolyte over time (Mason and Mackay 1976), and capacitive (Schwan 1966, Edelberg 1977) and non-linear (e.g. 'breakdown) responses to electrical current flow (Grimnes 1983). Given the very-long time course of tES (hundreds of seconds), time-dependent changes are not modeled here, while current-dependent effects are represented in the explored static conductivities.

Finally, depending on the fraction of current shunted through the skin and other anatomical factors, skin conductivity may impact current reaching the brain (Truong *et al* 2013, Opitz *et al* 2015, Saturnino *et al* 2015, 2019). Notably, there are three orders of magnitude variation in scalp conductivity values used across various tES modeling pipelines (Miranda *et al* 2006, Kuhn *et al* 2009, Opitz *et al* 2015, Gomez-Tames *et al* 2016), which in part reflects the known variation across layers of skin. One modeling study (with homogenous skin) suggested that brain current flow pattern may be impacted by current flow distribution at the electrode (Saturnino *et al* 2015). Proper consideration of current flow through skin may impact brain current flow during tES.

2. Methods

2.1. Computational model and solution method

2.1.1. Skin anatomy

Skin is a complex mosaic layer of tissues perforated by sweat ducts and hair follicles with different characteristics (Panescu *et al* 1993). It is made up of three primary layers namely epidermis, dermis, and subcutaneous/fat. Epidermis, the outermost layer of the skin, consists of predominantly keratin cells (dead cells) and its thickness ranges from 50–150 μm depending on body region (Kolarsick *et al* 2011, Yousef *et al* 2020). Sweat ducts are filled with sweat which has an electrical conductivity equivalent to 0.1–0.4% saline solution (Suchi 1955). The density of sweat glands varies across different skin regions (for example, on the forearm: ∼160 $cm^{-2;}$ on the palmer and planter surfaces of the hand and feet: ∼370 cm^{-2}) (Tregear 1966, Edelberg 1977). The most superficial layer of the epidermis is stratum corneum (10–15 μm thickness), a very poor conductor of electricity (Yamamoto and Yamamoto 1976). Dermis is the immediate layer under the epidermis and contains living cells with greater blood vessels density that provide nutrition to the skin and maintain thermoregulation (Luna *et al* 2015). The remaining tissue layer of the skin is subcutaneous and it consists of fat, adipose tissue, connective tissues, and muscles (Kolarsick *et al* 2011, Yousef *et al* 2020). All skin layers include nerves endings (sensors), synapses, and/or axons so current density patterns through each is considered (Arthur and Shelley 1959, Kennedy and Wendelschafer-Crabb 1993, Chateau and Misery 2004, Kolarsick *et al* 2011).

We modelled three classes of skin model: basic (homogeneous), intermediate (multi-layer with or without ultra-structures), and advanced (high-resolution with realistic anatomy). The basic skin model, like the prior skin model (Miranda *et al* 2006; Datta *et al* 2009b, Minhas *et al* 2011, Kronberg and Bikson 2012, Saturnino *et al* 2015), is a homogeneous block representing combined mass of the skin tissues. The intermediate model, which was adapted from our prior study (Khadka *et al* 2018b), represent the major skin layers (epidermis, dermis, and subcutaneous fat). We assessed the role of the skin ultra-structures by successively adding moderately-realistic (geometric shapes) hair follicles (diameter: 1 mm), sweat glands (diameter: 1 mm), and blood vessels (diameter: 10 mm) into the multi-layer skin model. Finally, based on the prediction from the multi-layer skin with moderately-realistic ultra-structures, we developed a high-resolution anatomically realistic and detailed skin model. The anatomical shape (mosaic pattern, folding, and ridge patterns (mainly in epidermis and dermis)), and dimensions (thickness and diameter) of multi-layer and ultra-structures were based on prior cadaver (Kolarsick *et al* 2011, Yousef *et al* 2020) and imaging data (Welzel 2001, Mogensen *et al* 2009, Olsen *et al* 2015, Hussain *et al* 2017). Specifically, the standard thickness of the epidermis, dermis, and fat were 0.1 mm, 2 mm, and 3 cm, respectively. The diameter of the hair follicles and sweat glands were 0.2 mm and 0.05 mm. The location of hair follicles and sweat glands were allocated arbitrarily and were seeded alternatively across the skin surface. We only modeled the lumen of blood vessels. The diameter of blood vessel was 0.12 mm and the intercapillary distance was 50 μm.

2.1.2. Model construction and computational method

All variations of the skin models were modeled as computer-aided design (CAD) files in SolidWorks (Dassault Systemes Americas Corp., MA, USA) and imported into Simpleware (Synopsys, CA, USA) to generate an adaptive tetrahedral mesh using a built-in voxel-based meshing algorithm. The models were refined to a finer mesh density until additional refinement produced less than 1% difference in predicted voltage at the surface of the skin. The resulting mesh consisted of >6 million (mesh size- min: 0.5 mm; max: 1 mm), >28 million (mesh size- min: 0.08 mm; max: 1 mm), >31 million (mesh size- min: 0.08 mm; max: 1 mm), >29 million (mesh size- min: 0.08 mm; max: 1 mm), and >70 million (mesh size- min: 0.02 mm; max: 1 mm) tetrahedral elements for homogeneous, multi-layer skin without ultra-structures, multi-layer skin with either hair follicles or sweat glands (moderately-realistic geometric shapes), multi-layer skin with only blood vessels (moderately-realistic geometric shapes), and high-resolution skin models, respectively. The models were imported into COMSOL Multiphysics 5.1 (COMSOL Inc. MA, USA) to computationally solve the FEM under steady-state assumption.

We defined standard conductivities for the skin layers and ultra-structures based on averaged value from prior literatures as: 1.05×10^{-5} S m^{-1} (epidermis); 0.23 S m^{-1} (dermis); 2×10^{-4} S m^{-1} (fat); 1.65×10^{-5} S m^{-1} (hair follicles); 1.4 S m^{-1} (sweat gland); and 0.7 S m^{-1} (blood vessels) (Yamamoto and Yamamoto 1976, Werner and Buse 1988, Wilson and Spence 1988, Hodson *et al* 1989, Duck 1990, Hua *et al* 1993, Torvi and Dale 1994, Panescu *et al* 1994a, Gabriel *et al* 1996, Pavšelj *et al* 2007, 2007, Wagner *et al* 2007, Sha *et al* 2008, Kuhn *et al* 2009, Çetingül and Herman 2010, Gomez-Tames *et al* 2016, Wake *et al* 2016, Khadka *et al* 2018b). For the homogeneous skin model, we assigned three isotropic electrical conductivities: standard epidermis conductivity: 1.05×10^{-5} S m^{-1}; moderate epidermis conductivity: 0.12 S m^{-1}; and

prior bulk skin conductivity: 0.465 S m^{-1} (Datta *et al* 2009b; Truong *et al* 2013, Leite *et al* 2018). For the multi-layer skin model without ultra-structures, we assigned two epidermis (1.05×10^{-5} S m^{-1}, 0.12 S m^{-1}) and dermis (0.23 S m^{-1}, 1.05×10^{-5} S m^{-1}) conductivities while the fat conductivity remain unchanged (2×10^{-4} S m^{-1}) (figure 2), and for model with ultra-structures, we assigned standard epidermis (1.05×10^{-5} S m^{-1}), dermis (0.23 S m^{-1}), and fat (2×10^{-4} S m^{-1}) conductivities (figure 3). We further simulated a range of skin multi-layer tissue thickness (by halving and doubling the thickness of the standard multi-layer model) to consider the impact of varied scalp locations used in tES montages, as well as an arched multi-layer skin model with mosaic pattern across the skin layers to consider the impact of realistic scalp/skin curvature of the head. Unless otherwise stated, multi-layer simulations had standard flat surfaces. Two variants of epidermis conductivities (standard (1.05×10^{-5} S m^{-1}) and moderate (0.12 S m^{-1})) and three variants of dermis conductivities (standard (0.23 S m^{-1}), minimum (0.0023 S m^{-1}), and maximum (23 S m^{-1})) were assigned to the high resolution skin model (figure 4). In sum, a total of 78 variations of skin layer conductivities were simulated. We modeled two sponge electrode types- thin (3.8 mm thickness) and thick (5.6 mm thickness). Unless otherwise stated, we simulated flat-shaped thick sponge electrode (1.4 S m^{-1}).

For the boundary conditions, a static inward normal current density (J_{norm}) corresponding to 1 mA was applied through the top exposed surface of the sponge electrode (for both electrode types) positioned dorsal to the skin voxel while the ventral surface of the skin voxel was grounded, with the remaining external boundaries electrically insulated. Models were constructed such that current density was insensitive to the modeled tissue exterior boundary size. The Laplace equation ($\nabla(\sigma\nabla V) = 0$) for voltage (and in turn electric field and current density) was applied and solved as the field equations to determine the current densities at different skin layers and ultra-structures. Predicted current density plots were sampled 10 μm below the epidermis, dermis, and fat for all skin model variations. Average current densities for each skin layers were sampled from a 1 cm × 1 cm ROI defined at the edge and the center of the pad. The ROI excludes current density across or at the perimeter of the ultra-structures. The spatial current density profile was quantified at each skin layers by sampling the predicted current density diagonally (edge-to-edge) and normalizing the local current density to the maximum current density within either of the ROIs. The coefficient of annularity of current density distribution (κ) was quantified as a ratio between the averaged current density at the edge vs current density at the center of the sponge pad ($\kappa = J_{edge}/J_{center}$) for each layers where $\kappa \leq 1$ was accepted as a non-annular pattern otherwise considered as an annular ($\kappa > 1$).

3. Results

3.1. Current flow in a homogeneous skin with varied conductivities

To understand the role of electrical properties of skin in current flow pattern, we first modeled a homogeneous skin model with varied electrical conductivity (figure 1). We considered three electrical conductivities of homogenous skin- (1) standard epidermis conductivity (1.05×10^{-5} S m^{-1}, figure 1(C1)); (2) moderate epidermis conductivity (0.12 S m^{-1}, figure 1(C2)); and (3) prior bulk skin conductivity (0.465 S m^{-1}, figure 1(C3)). Compared to the prediction of prior bulk skin conductivity model (figure 1(C3)), the peak current densities (at the electrode edges) predicted by the moderate epidermis conductivity skin and the standard epidermis conductivity skin were ∼8% and ∼11% lower (figure 1(C1), (C2), (C3)), respectively. However, all homogenous model variations predicted an annular current density distribution at the surface of the skin ($\kappa = 26.62$ (standard epidermis conductivity); $\kappa = 27.51$ (moderate epidermis conductivity); and $\kappa = 29.70$ (prior bulk skin conductivity) figure 1(B), C1, C2, C3).

3.2. Role of skin multi-layer in current flow

We adapted the previously developed multi-layer skin model (Khadka *et al* 2018b) and predicted the role of skin layers with varied electrical conductivities on current flow patterns through the skin (figure 2(A)). We first compared the model prediction by considering two epidermis conductivities (standard:1.05×10^{-5} S m^{-1} and moderate: 0.12 S m^{-1}), and two dermis conductivities (standard dermis: 0.23 S m^{-1} and standard epidermis value: 1.05×10^{-5} S m^{-1}) and standard fat conductivity (2×10^{-4} S m^{-1}) (figures 2(C), (D), (E)). The standard conductivity multi-layer skin model predicted an annular current density pattern ($\kappa = 1.41$) in the epidermis layer (figure 2(C)). The multi-layer skin model with moderate epidermis conductivity, and standard dermis and fat conductivity (figure 2(D)), as well as the model with low epidermis (standard value) and dermis (standard epidermis value) conductivity, and standard fat conductivity (figure 2(E)) models also predicted an annular current density pattern at the electrode edges in the epidermis ($\kappa = 305$ and $\kappa = 12.51$). In the dermis layer, current density pattern remained annular at the electrode edges for all conductivity variations ($\kappa = 8.21$, $\kappa = 212.50$, $\kappa = 4.45$, respectively), however in the fat layer, current density edge effect was eliminated (non-annular pattern) in

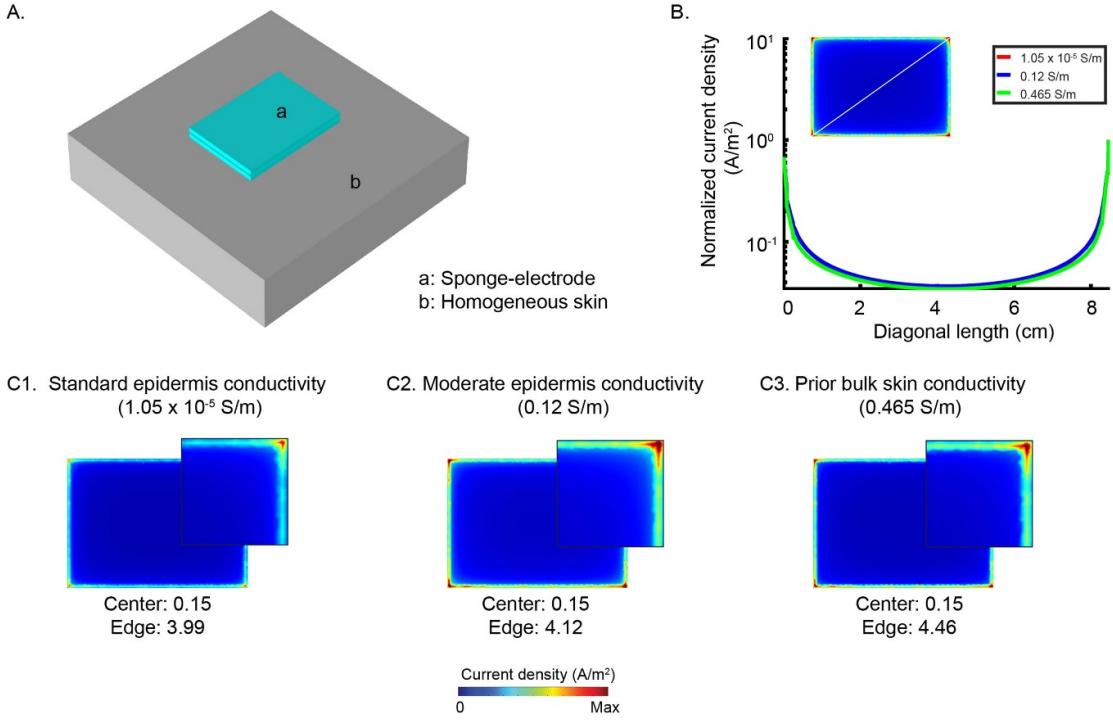

Figure 1. Homogenous skin model and current flow. (A) Illustration of a homogeneous skin model with conventional tDCS electrode. (B1) Diagonal (edge-to-edge, white line) current density plot, normalized to the peak current density (at the edge) for standard epidermis conductivity (1.05×10^{-5} S m^{-1}), moderate epidermis conductivity (0.12 S m^{-1}), and prior bulk skin conductivity (0.465 S m^{-1}) (color coded). (C1, C2, and C3) represent predicted current density plots sampled 10 μm below the surface of skin for the three variants of skin electrical conductivity. Current density across conditions at the skin surface was annular ($\kappa > 1$).

the standard skin layers conductivities ($\kappa = 0.95$), and moderate epidermis conductivity and standard dermis and fat conductivity models ($\kappa = 0.98$), except for the low epidermis (standard value) and dermis (standard epidermis value) conductivity and standard fat conductivity model ($\kappa = 1.50$) (figures 2(C), (D), (E)). In the multi-layer skin model without ultrastructure, under no conductivity combinations did we predict a non-annular current density pattern at both epidermis and dermis.

In order to consider variation in skin layers thickness as may vary across different scalp location and among subjects, we simulated a range of skin multi-layer thickness by halving and doubling the standard tissue thickness. The current flow pattern through the skin was insensitive to the multi-layer thickness (figure not shown). Halving and doubling the skin multi-layer thickness resulted in predictions of comparable κ value (annularity) at both epidermis and dermis as the standard conductivity multi-layer skin model (halving: epidermis ($\kappa = 1.52$), dermis ($\kappa = 8.93$); fat ($\kappa = 0.88$); doubling: (epidermis ($\kappa = 1.47$), dermis ($\kappa = 4.27$); fat ($\kappa = 1.0$)).

Mimicking the realistic anatomy of the human head, we also simulated a curvature skin/scalp multi-layer model and assessed the role of curvature in current flow. Addition of curvature into the multi-layer skin model produced similar predictions of an annular pattern at both epidermis and dermis layers (epidermis ($\kappa = 1.88$), dermis ($\kappa = 5.98$)).

Expanding on the above, we conducted a sensitivity analysis considering various combinations of skin layers electrical conductivities, to specifically consider under which parameters current is non-annular across all skin layers. Here we simulated a thin sponge electrode. Altogether, 65 variant of electrical conductivity (S m^{-1}) combinations of epidermis (standard: 1.05×10^{-5}; range: 1.05×10^{-3} to 1.05×10^{-6} and moderate: 0.12; range: 0.0012 to 12), dermis (standard: 0.23; range: 0.0023 to 23), and fat (standard: 2×10^{-4}; range: 0.02 to 2×10^{-5}) were simulated. None of the conductivity combination resulted in a prediction of non-annular current density pattern ($\kappa > 1$) at both epidermis and dermis—only 17 conductivity combinations (reduced epidermis conductivity and/or increased dermis conductivity) resulted in a non-annular pattern ($\kappa \leq 1$) in the epidermis (results not shown).

3.3. Role of skin multi-layer and isolated ultrastructures in current flow

Multi-layer alone did not address current flow pattern through the skin. Therefore, we modeled hair follicles, sweat glands, and blood vessels within the multi-layer skin model. In this section, we start by modeling each

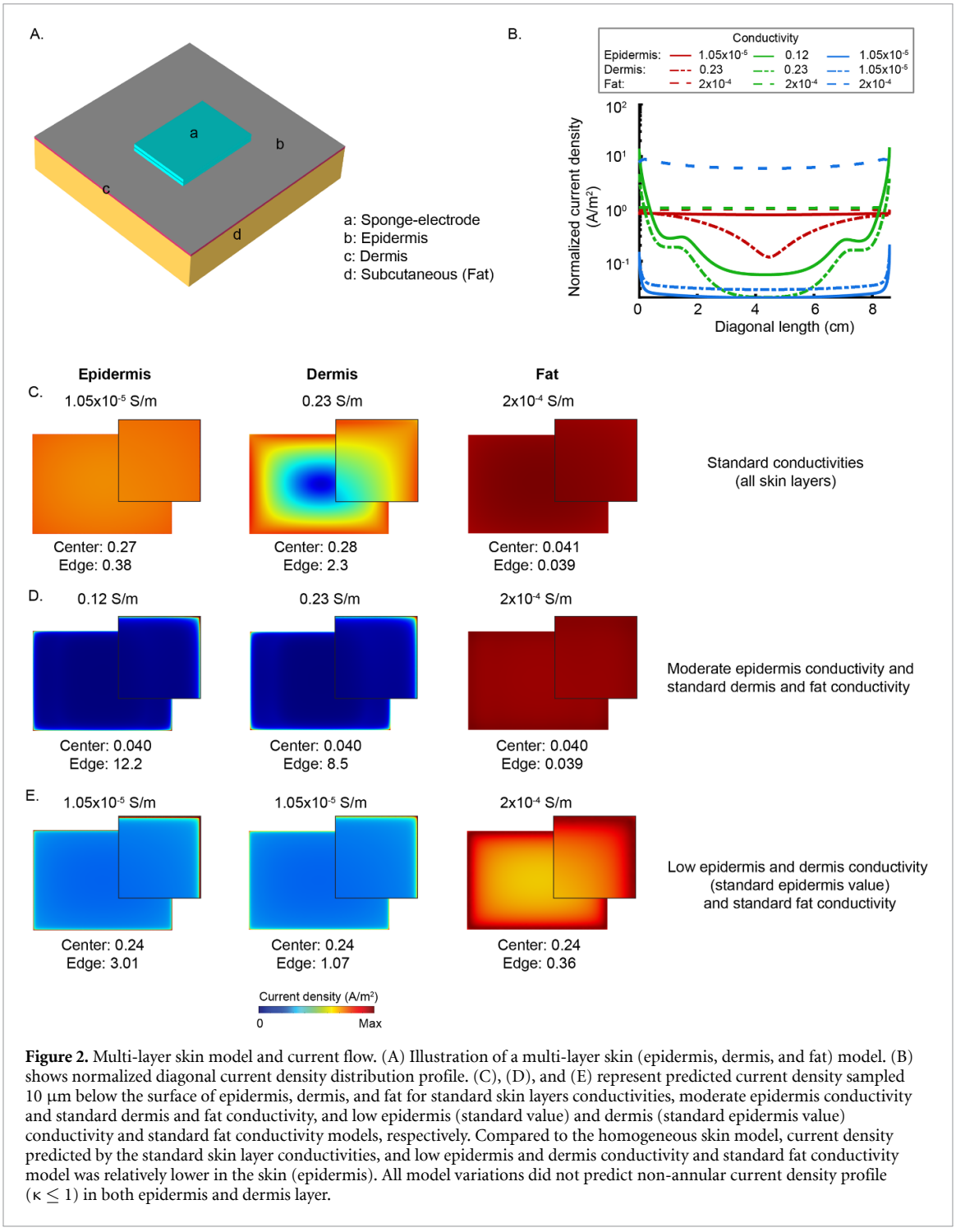

Figure 2. Multi-layer skin model and current flow. (A) Illustration of a multi-layer skin (epidermis, dermis, and fat) model. (B) shows normalized diagonal current density distribution profile. (C), (D), and (E) represent predicted current density sampled 10 μm below the surface of epidermis, dermis, and fat for standard skin layers conductivities, moderate epidermis conductivity and standard dermis and fat conductivity, and low epidermis (standard value) and dermis (standard epidermis value) conductivity and standard fat conductivity models, respectively. Compared to the homogeneous skin model, current density predicted by the standard skin layer conductivities, and low epidermis and dermis conductivity and standard fat conductivity model was relatively lower in the skin (epidermis). All model variations did not predict non-annular current density profile ($\kappa \leq 1$) in both epidermis and dermis layer.

ultra-structure in isolation, with a geometric shapes (diameter of sweat gland and hair follicle: 1 mm, and blood vessels: 10 mm), and using the standard epidermis (1.05×10^{-5} S m^{-1}), dermis (0.12 S m^{-1}), and fat (2×10^{-4} S m^{-1}) conductivities.

In the epidermis and fat layers, addition of only hair follicles (figure 3(D)) into the multi-layer skin model resulted in a prediction of lower current density at the electrode edges compared to the center (non-annular: $\kappa = 0.59$), and higher current density around the outer perimeter of the resistive hair follicles. However, current density in the dermis layer was higher at the electrode edges compared to the center ($\kappa = 4.93$), though still lower than the current density peaks around the hair follicles. In this case, in the fat layer current density was non-annular ($\kappa = 0.97$).

When only sweat glands was added into the multi-layer skin (figure 3(E)), the model resulted in a prediction of an annular current density pattern in the epidermis ($\kappa = 1.25$), with punctate peak current

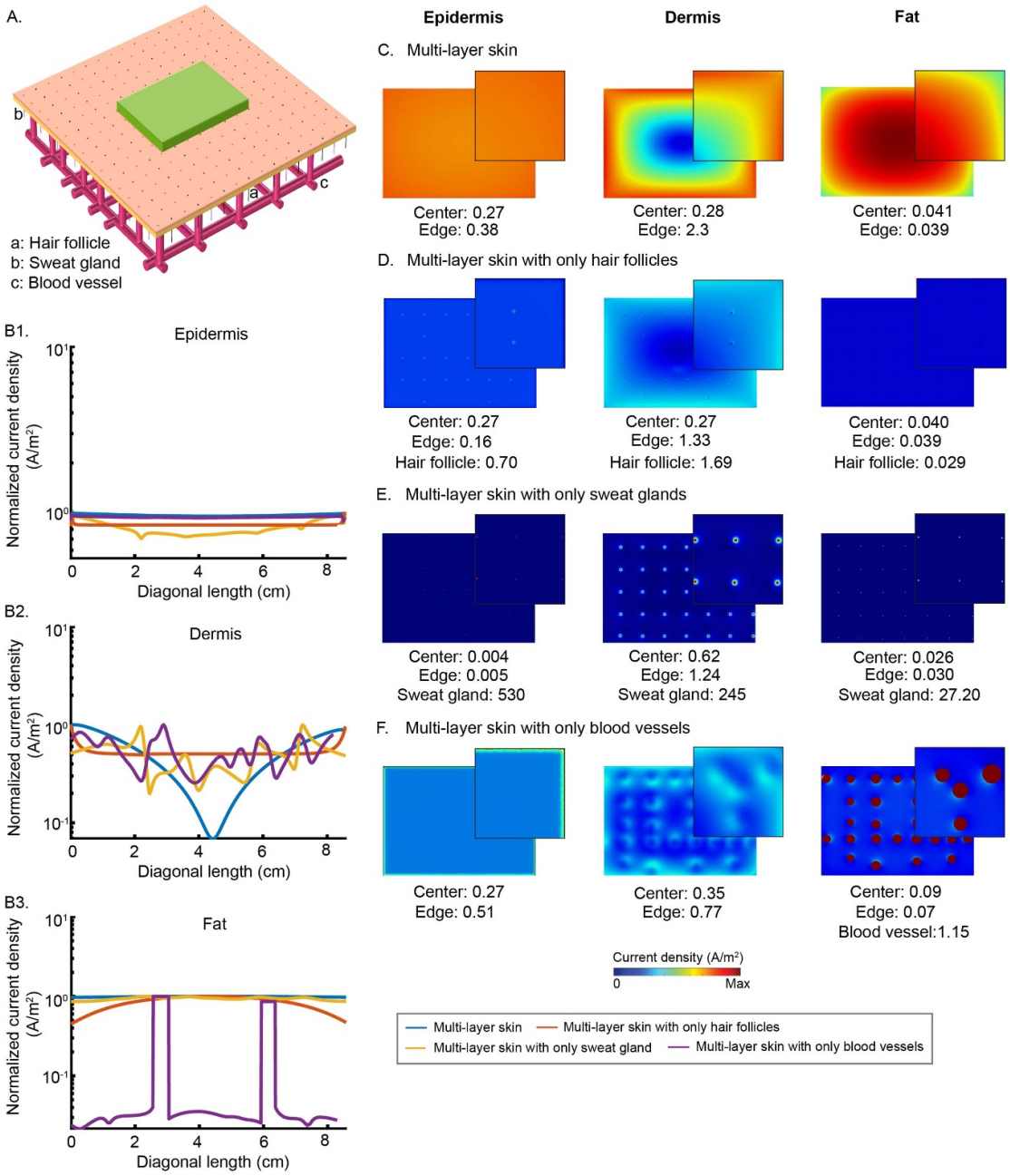

Figure 3. Successive addition of moderately-realistic skin ultra-structures (hair follicles, sweat glands, and blood vessels) into the multi-layer skin model. (A) represents multi-layer skin model with sweat glands, hair follicles, and blood vessels. (B1, B2, B3) shows normalized current density distribution in the epidermis, dermis, and fat for model variations. (C) shows current density plots for multi-layer skin model without ultra-structures. (D) represents current density prediction with the addition of only hair follicles. Reported current density is around the outer perimeter of the hair follicle. (E) represents current flow pattern with the addition of only sweat glands, and (F) with the addition of only blood vessels into the multi-layer skin model. Sweat glands and blood vessels provides conductive pathway for transcutaneous current flow to deeper skin layers, reflected by uniform current density across them.

density around the sweat glands in both epidermis (530 A m^{-2}) and dermis (245 A m^{-2}). These current density hotspots were consistent across sweat glands, both near and far from the electrode edges. In the fat layer, the current density pattern was annular ($\kappa = 1.15$) with the hotspots mainly under the sweat glands.

Addition of only blood vessels into the multi-layer skin model (figure 3(F)) resulted in a prediction of an annular current density pattern in the epidermis ($\kappa = 1.88$) and dermis ($\kappa = 2.20$). However, in the fat layer, current density edge effect was eliminated (non-annular; $\kappa = 0.77$). Notably, current density across the blood vessels was uniform under the electrode, both near and far from the electrode edges. Normalized current density plots show that sweat glands and blood vessels influence current flow pattern across skin layers (figure 3(B1), (B2), (B3)).

3.4. Role of anatomically realistic and detailed skin multi-layer and ultrastructures in current flow

We developed the first high-resolution anatomically realistic and detailed skin model to assess how the realistic tissue layers and multiple ultra-structures fundamentally change current flow pattern depending upon the parameters. For each layer, we report the maximum current density which is predicted across sweat glands in epidermis and dermis layer, and across blood vessel in fat layer.

We simulated the realistic skin model with four variants of electrical conductivities of the epidermis and dermis. With moderate epidermis conductivity (0.12 S m^{-1}) and standard dermis conductivity (0.23 S m^{-1}) (figure 4(B1)), the general current density pattern across the epidermis and dermis layer was annular (higher at the electrode edges compared to the center) in both epidermis ($\kappa = 13.51$) and dermis layer ($\kappa = 6.52$). Current concentration peaked in sweat glands in both epidermis and dermis layer. In the fat layer, the current density edge effect was eliminated (non-annular: $\kappa = 0.66$) and the hotspots were localized under sweat glands and across blood vessels. The realistic model with standard epidermis conductivity and maximum dermis conductivity model (figure 4(B2)) predicted a non-annular current density in the epidermis ($\kappa = 0.76$) and slightly annular distribution in the dermis ($\kappa = 1.09$), with the localized hotspots at sweat glands across both layers. The current density in the fat layer was lower at the edges compared to the center (non-annular: $\kappa = 0.77$), with hotspots under the sweat glands and across blood vessels. The standard epidermis conductivity and minimum dermis conductivity model (figure 4(B3)) resulted in a similar prediction of current density pattern in the epidermis, dermis, and fat layer, and across sweat glands and blood vessels as in the standard epidermis conductivity and maximum dermis conductivity model.

The standard epidermis and dermis conductivity model (figure 4(B4)) predicted non-annular current density in the epidermis ($\kappa = 1.0$) and fat layers ($\kappa = 0.46$), but an annular pattern in the dermis layer ($\kappa = 2.33$). In both epidermis and dermis layers, local maximum current densities were predicted across the sweat glands, and in the fat layer, current density was chiefly concentrated across the blood vessels and sweat glands. The normalized current density profiles in the epidermis was comparable for all the conductivity variation models (figure 4(C1)), except for the moderate epidermis conductivity and standard dermis conductivity. Note that the current density fluctuations across skin layers were due to the mosaic morphology of epidermis and dermis, and the ideocratic presence of the sweat glands, hair follicles, and blood vessels along the plotted current density trajectory (current density is higher across sweat gland and blood vessel, and around hair follicles) (figure 4(C1), (C2), (C3)). Overall, the results show that anatomically realistic skin multi-layer and ultra-structures can fundamentally change the current flow pattern depending upon the electrical conductivities.

4. Discussion

Applications of non-invasive electrical stimulation are very broad and long-standing, with most low-intensity (few mA peak) medical forms well tolerated. Regardless of whether the target is superficial, deep tissue, or transcranial, maximum current densities are inevitably generated at the skin. Adverse events are often minor and reflect reactions at the skin (e.g. tinging). Efforts to enhance deployability (e.g. dry electrodes; (Khadka *et al* 2018a)), support higher current (Khadka *et al* 2019, Reckow *et al* 2018, Workman *et al* 2020), or otherwise further enhance tolerability and thus focus on skin effects. Skin effects can result from electrochemical reactions at the electrode if they reach the skin surface (Merrill *et al* 2005, Minhas *et al* 2010) and from current flow through the skin. Skin is a complex non-linear mosaic structure and studies characterizing and modeling current flow through skin date back decades (Hua *et al* 1993, Panescu *et al* 1994a, 1994b, Miranda *et al* 2006, Kuhn *et al* 2009, Datta *et al* 2009b, Arena *et al* 2011, Medina and Grill 2014, Gholami-Boroujeny *et al* 2015, 2015, Gomez-Tames *et al* 2016, Khadka *et al* 2018b). Nonetheless, here we produce novel insight into questions not heretofore fully addressed, and also develop the first anatomically precise model of skin current flow.

On the one hand, minimization of current concentration that is predicted to occur around electrode edges (i.e. annular current density pattern) is a long-standing goal (Kim *et al* 1990, Wei and Grill 2005, Wang *et al* 2014, Sathi and Hosain 2020), including for transcutaneous electrical stimulation (Krasteva and Papazov 2002, Gilad *et al* 2007, Kronberg and Bikson 2012, Gomez-Tames *et al* 2016). On the other hand, we speculated that the experimental findings from transcutaneous stimulation are inconsistent with current flow concentration at the electrode edges (e.g. uniform erythema;(Dusch *et al* 2007, 2009, Ezquerro *et al* 2017)). *A priori*, we speculated that development of skin current flow models with increased detail and appropriate parameterization would predict uniform current flow. To this end, we conducted and extensive parameter sweep (figures 2, 3) and developed the first realistic FEM model of skin current flow (figure 4).

We conclude that no realistic parameterization of skin tissue layer conductivities in the absence of skin-ultrastructure or with the presence of a single geometric ultrastructure will produce uniform bulk current flow (not annular) pattern through both epidermis and dermis. Though plausible tissue parameters

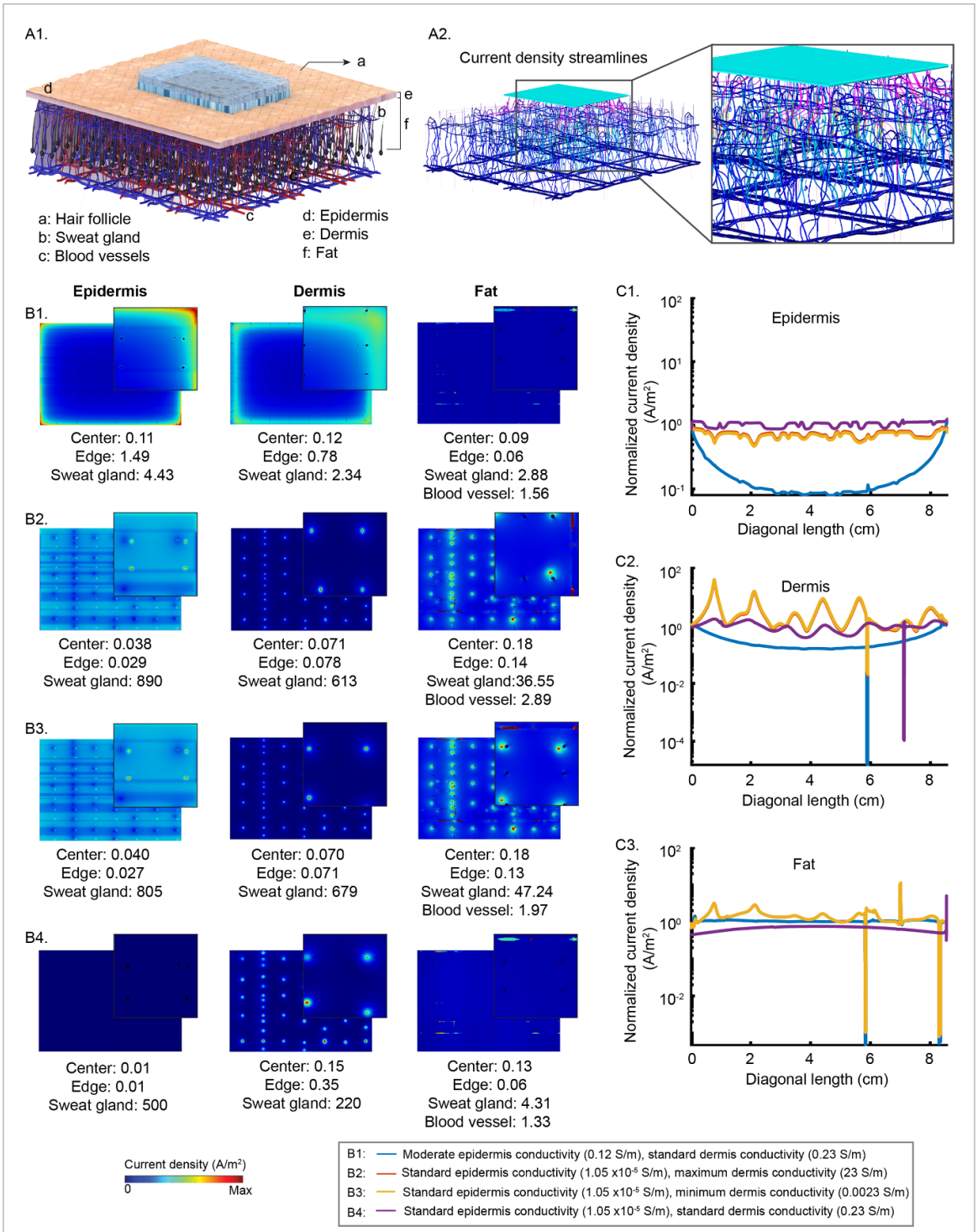

Figure 4. High-resolution anatomically realistic and detailed skin model and the current flow prediction. (A1) Illustration of the realistic skin model with detailed skin layers (mosaic morphology), hair follicles, sweat glands, and blood vessels. (A2) Current flow from electrode to deeper tissues with inset showing current density streamlines through the blood vessels and the sweat glands. (B1, B2, B3, B4) predicted current density in the epidermis, dermis, and fat under varied epidermis and dermis electrical conductivities. Moderate epidermis conductivity and standard dermis conductivity model predicted an annular current density pattern in epidermis and dermis ($\kappa > 1$), and non-annular profile in fat layer ($\kappa \leq 1$). (B1) Standard epidermis conductivity but varied dermis conductivities (maximum: 23 S m^{-1} and minimum: 0.0023 S m^{-1}) predicted non-annular current density profile in the epidermis and fat ($\kappa \leq 1$), and annular in the dermis ($\kappa > 1$). (B2, B3) Standard epidermis and dermis conductivity model predicted non-annular current density in the epidermis and fat ($\kappa \leq 1$) but annular in dermis ($\kappa > 1$). (B4) Current flow across the sweat gland and blood vessels were uniform (current density hotspot around sweat gland and blood vessels) and concentrated around the hair follicles across (not reported) all simulation variations. (C1, C2, C3) represent normalized current density profile at the epidermis, dermis, and fat, respectively. Noticeable fluctuations in current density at the epidermis and dermis emphasizes the influence of skin anatomy and ultra-structures in skin current flow pattern.

can reduce current concentration around the electrode edges, namely reduced epidermis conductivity and increased/reduced dermis conductivity (figure 4(B2), (B3)). We also confirm prior effort using geometric representation of skin hair follicles and sweat glands (Gomez-Tames *et al* 2016), that presence of these ultrastructure result in punctate peaks in current flow; however, we show an annular pattern remains in the skin bulk for all realistic parameters. We modeled a vascular network for the first time and predict a high and uniform current density across the vascular network (i.e. not concentrated near electrode edges); a result consistent with uniform erythema observed experimentally.

Only a model incorporating realistic skin anatomy and ultrastructure resulted in predictions of largely uniform bulk current flow across skin layers under the electrode. To the extent current was annular under some tissue parameters, it was only modestly so, and in some cases current density was in fact higher near the electrode center ($\kappa \leq 1$).

Prior simulations that current concentrate around electrode edges is consistent across a broad range of skin parameters, electrode shapes, sizes, and separation, and flat, circular, or realistic anatomy (Krasteva and Papazov 2002, Faria *et al* 2011, Minhas *et al* 2011, Khadka *et al* 2015, Saturnino *et al* 2015). For example, in two studies electrode sizes spanning 3 to 25 cm^2, electrode separation spanning 2.5 to ~10 cm, with placement across the scalp, spanning varied pediatric and adult heads, and varied scalp thickness and fat content (e.g. obese), predicted an annular skin current flow (Kessler *et al* 2013, Truong *et al* 2013), consistent with the prediction of our multi-layer skin model with varied thickness and curvature. Across modeling studies, the proximity of the counter electrode has negligible or little impact on skin current flow pattern (Kessler *et al* 2013, Truong *et al* 2013, Saturnino *et al* 2015) and current density is largely symmetric around electrodes (Kessler *et al* 2013, Truong *et al* 2013)—these aspects also support the use of a generic return boundary condition in our simulation and other skin models (Krasteva and Papazov 2002, Sha *et al* 2008, Kronberg and Bikson 2012, Gomez-Tames *et al* 2016). Our fundamental proposition that current flow models without ultra-structures predict a highly annular skin current flow pattern is robust and reinforced here through the broad range of multi-layer skin parameters modeled here (figure 3). In this same sense, we suggest that our finding that addition of ultra-structures were necessary to produce a uniform current flow through epidermis and dermis should generalize across a range of electrode configurations.

The frequency and current dependent impedance of skin (and its various layers and structures) has been exhaustively studied (Tregear 1965, Carter and Morley 1969, Lykken 1970, Yamamoto and Yamamoto 1977, Woo *et al* 1992, Martinsen *et al* 1997, Dorgan and Reilly 1999, Huclova *et al* 2012, Luna *et al* 2015). When impedance decreases with frequency, compartments of the skin are modeled as a dielectric (capacitor in lumped parameter models) (Yamamoto and Yamamoto 1976, Grimnes 1983, Gabriel *et al* 1987, Martinsen *et al* 1997). Increasingly complex skin responses are represented with various non-linear models to stimulation frequency, current, exposure time, and environment conditions (Suchi 1955, Schwan 1966, Mason and Mackay 1976, Edelberg 1977, Grimnes 1983, Pierard-Franchimont and Pierard 2015). Nonetheless, for any given instant, skin current flow can be modeled by the effective resistivity of each compartment. Therefore, varying the resistivity of skin compartments, as done here, allows considering a range of possible current intensities, waveforms, and exposure conditions. Thus, we consider our conclusion that ultra-structure is essential for non-annular skin current flow patterns generalizable across waveforms and exposure conditions since multi-layer model failed to produce a uniform current flow across resistivities tested.

Taken together, they suggest that precise representation of skin anatomy fundamentally impacts predicted current flow patterns: (1) consistent with prior models, presence of hair follicles or sweat glands produces punctate current density peaks; (2) we show that consideration of blood vessels produces uniform current, maximum across the vascular network; (3) only a model with complete anatomical detail predicted absence of current concentration near electrode edges across all skin layers.

Acknowledgments

Source(s) of financial support: This study was partially funded by grants to MB from NIH (NIH-NIMH 1R01MH111896, NIH-NINDS 1R01NS101362, NIH-NCI U54CA137788/U54CA132378, R03 NS054783) New York State Department of Health (NYS DOH, DOH01-C31291GG), and cycle 50 PSC-CUNY.

Conflict of interest

The City University of New York (CUNY) has IP on neuro-stimulation systems and methods with authors NK and MB as inventors. MB has equity in Soterix Medical. MB served on the advisory boards and/or consulted for Boston Scientific, Mecta, Halo Neuroscience, and GlaxoSmithKline Inc.

ORCID iD

Niranjan Khadka https://orcid.org/0000-0002-4930-5214

References

Adair D *et al* 2020 Electrical stimulation of cranial nerves in cognition and disease *Brain Stimul.* **13** 717–50

Ambrus G G, Antal A and Paulus W 2011 Comparing cutaneous perception induced by electrical stimulation using rectangular and round shaped electrodes *Clin. Neurophysiol.* **122** 803–7

Antal A *et al* 2017 Low intensity transcranial electric stimulation: safety, ethical, legal regulatory and application guidelines *Clin. Neurophysiol.* **128** 1774–809

Aparício L V M, Guarienti F, Razza L B, Carvalho A F, Fregni F and Brunoni A R 2016 A systematic review on the acceptability and tolerability of transcranial direct current stimulation treatment in neuropsychiatry trials *Brain Stimul.* **9** 671–81

Arena C B, Sano M B, Rylander M N and Davalos R V 2011 Theoretical considerations of tissue electroporation with high-frequency bipolar pulses *IEEE Trans. Biomed. Eng.* **58** 1474–82

Arthur R P and Shelley W B 1959 The innervation of human epidermis *J. Investigative Dermatology* **32** 397–411

Asamoah B, Khatoun A and Mc Laughlin M 2019 tACS motor system effects can be caused by transcutaneous stimulation of peripheral nerves *Nat. Commun.* **10** 266

Bikson M, Datta A and Elwassif M 2009 Establishing safety limits for transcranial direct current stimulation *Clin. Neurophysiol.* **120** 1033–4

Bikson M *et al* 2016 Safety of transcranial direct current stimulation: evidence based update 2016 *Brain Stimul.* **9** 641–61

Bikson M *et al* 2018 Limited output transcranial electrical stimulation (LOTES-2017): engineering principles, regulatory statutes, and industry standards for wellness, over-the-counter, or prescription devices with low risk *Brain Stimul.* **11** 134–57

Carter A O and Morley R 1969 Electric current flow through human skin at power frequency voltages *Br. J. Ind. Med.* **26** 217–23

Çetingül M P and Herman C 2010 A heat transfer model of skin tissue for the detection of lesions: sensitivity analysis *Phys. Med. Biol.* **55** 5933

Chateau Y and Misery L 2004 Connections between nerve endings and epidermal cells: are they synapses? *Exp. Dermatol.* **13** 2–4

Datta A, Elwassif M and Bikson M 2009a Bio-heat transfer model of transcranial DC stimulation: comparison of conventional pad versus ring electrode *2009 Annual Int. Conf. of the IEEE Engineering in Medicine and Biology Society* EMBC 2009 pp 670–3

Datta A, Bansal V, Diaz J, Patel J, Reato D and Bikson M 2009b Gyri-precise head model of transcranial direct current stimulation: improved spatial focality using a ring electrode versus conventional rectangular pad *Brain Stimul.* **2** 201–7

Dorgan S J and Reilly R B 1999 A model for human skin impedance during surface functional neuromuscular stimulation *IEEE Trans. Rehabil. Eng.* **7** 8

Duck F A 1990 *Physical Properties of Tissue: A Comprehensive Reference Book* (New York: Academic)

Dundas J E, Thickbroom G W and Mastaglia F L 2007 Perception of comfort during transcranial DC stimulation: effect of NaCl solution concentration applied to sponge electrodes *Clin. Neurophysiol.* **118** 1166–70

Dusch M, Schley M, Obreja O, Forsch E, Schmelz M and Rukwied R 2009 Comparison of electrically induced flare response patterns in human and pig skin *Inflamm. Res.* **58** 639–48

Dusch M, Schley M, Rukwied R and Schmelz M 2007 Rapid flare development evoked by current frequency-dependent stimulation analyzed by full-field laser perfusion imaging *Neuroreport* **18** 1101–5

Edelberg R 1977 Relation of electrical properties of skin to structure and physiologic state *J. Investigative Dermatology* **69** 324–7

Ezquerro F *et al* 2017 The influence of skin redness on blinding in transcranial direct current stimulation studies: a crossover trial *Neuromodulation: Technol. Neural Interface* **20** 248–55

Faria P, Hallett M and Miranda P C 2011 A finite element analysis of the effect of electrode area and inter-electrode distance on the spatial distribution of the current density in tDCS *J. Neural Eng.* **8** 066017

Fertonani A, Ferrari C and Miniussi C 2015 What do you feel if I apply transcranial electric stimulation? Safety, sensations and secondary induced effects *Clin. Neurophysiol.* **126** 2181–8

Fonteneau C *et al* 2019 Sham tDCS: a hidden source of variability? Reflections for further blinded, controlled trials *Brain Stimul.* **12** 668–73

Gabriel C, Bentall R H and Grant E H 1987 Comparison of the dielectric properties of normal and wounded human skin material *Bioelectromagnetics* **8** 23–27

Gabriel S, Lau R W and Gabriel C 1996 The dielectric properties of biological tissues: III. Parametric models for the dielectric spectrum of tissues *Phys. Med. Biol.* **41** 2271

Geldard F A 1974 *Conf. on Cutaneous Communication Systems and Devices* (*Sponsored Jointly by the Advanced Research Projects Agency of the U.S. Dept. of Defense and the Office of Naval Research and Held at the Royal Inn, Monterey California, on April 17–18, 1973*) (Psychonomic Society)

Gholami-Boroujeny S, Mekonnen A, Batkin I and Bolic M 2015 Theoretical analysis of the effect of temperature on current delivery to the brain during tDCS *Brain Stimul.* **8** 509–14

Gilad O, Horesh L and Holder D S 2007 Design of electrodes and current limits for low frequency electrical impedance tomography of the brain *Med. Bio. Eng. Comput.* **45** 621–33

Gomez-Tames J, Sugiyama Y, Laakso I, Tanaka S, Koyama S, Sadato N and Hirata A 2016 Effect of microscopic modeling of skin in electrical and thermal analysis of transcranial direct current stimulation *Phys. Med. Biol.* **61** 8825

Greinacher R, Buhôt L, Möller L and Learmonth G 2018 The time course of ineffective sham blinding during 1mA tDCS (arXiv:462424)

Grimnes S 1983 Dielectric breakdown of human skin in vivo *Med. Biol. Eng. Comput.* **21** 379–81

Hahn C, Rice J, Macuff S, Minhas P, Rahman A and Bikson M 2013 Methods for extra-low voltage transcranial direct current stimulation: current and time dependent impedance decreases *Clin. Neurophysiol.* **124** 551–6

Hodson D A, Barbenel J C and Eason G 1989 Modelling transient heat transfer through the skin and a contact material *Phys. Med. Biol.* **34** 1493

Hua P, Woo E J, Webster J G and Tompkins W J 1993 Finite element modeling of electrode-skin contact impedance in electrical impedance tomography *IEEE Trans. Biomed. Eng.* **40** 335–43

Huclova S, Erni D and Fröhlich J 2012 Modelling and validation of dielectric properties of human skin in the MHz region focusing on skin layer morphology and material composition *J. Phys. D: Appl. Phys.* **45** 025301

Hussain A A, Themstrup L, Mogensen M and Jemec G B E 2017 Optical Coherence Tomography Imaging of the Skin *Agache's Measuring the Skin: Non-Invasive Investigations, Physiology, Normal Constants*, eds P Humbert, F Fanian, H I Maibach and P Agache (Cham: Springer International Publishing) pp 493–502
Kennedy W R and Wendelschafer-Crabb G 1993 The innervation of human epidermis *J. Neurol. Sci.* **115** 184–90
Kessler S K, Minhas P, Woods A J, Rosen A, Gorman C and Bikson M 2013 Dosage considerations for transcranial direct current stimulation in children: a computational modeling study *PloS One* **8** e76112
Kessler S K, Turkeltaub P E, Benson J G and Hamilton R H 2012 Differences in the experience of active and sham transcranial direct current stimulation *Brain Stimul.* **5** 155–62
Khadka N *et al* 2019 Adaptive current tDCS up to 4 mA *Brain Stimul.* **13** 69–79
Khadka N, Borges H, Zannou A L, Jang J, Kim B, Lee K and Bikson M 2018a Dry tDCS: tolerability of a novel multilayer hydrogel composite non-adhesive electrode for transcranial direct current stimulation *Brain Stimul.* **11** 1044–53
Khadka N, Truong D Q and Bikson M 2015 Principles of within electrode current steering *J. Med. Devices* **9** 020947–020947–2
Khadka N, Zannou A L, Zunara F, Truong D Q, Dmochowski J and Bikson M 2018b Minimal heating at the skin surface during transcranial direct current stimulation *Neuromodulation* **21** 334–9
Kim Y, Zieber H G and Wang F E 1990 Uniformity of current density under stimulating electrodes *Crit. Rev. Biomed. Eng.* **17** 585–619
Kolarsick P A J, Kolarsick M A and Goodwin C 2011 Anatomy and physiology of the skin *J. Dermatology Nurses' Assoc.* **3** 203
Krasteva V T and Papazov S P 2002 Estimation of current density distribution under electrodes for external defibrillation *Biomed. Eng. Online* **1** 7
Kronberg G and Bikson M 2012 Electrode assembly design for transcranial Direct Current Stimulation: a FEM modeling study *Conf. Proc. IEEE Eng. Med. Biol. Soc.* **2012** 891–5
Kuhn A, Keller T, Lawrence M and Morari M 2009 A model for transcutaneous current stimulation: simulations and experiments *Med. Biol. Eng. Comput.* **47** 279–89
Leite J, Gonçalves Ó F, Pereira P, Khadka N, Bikson M, Fregni F and Carvalho S 2018 The differential effects of unihemispheric and bihemispheric tDCS over the inferior frontal gyrus on proactive control *Neurosci. Res.* **130** 39–46
Luna J L V, Krenn M, Ramírez J A C and Mayr W 2015 Dynamic impedance model of the skin-electrode interface for transcutaneous electrical stimulation *PloS One* **10** e0125609
Lykken D T 1970 Square-wave analysis of skin impedance *Psychophysiology* **7** 262–75
Martinsen O G, Grimnes S and Sveen O 1997 Dielectric properties of some keratinised tissues. Part 1: stratum corneum and nail in situ *Med. Biol. Eng. Comput.* **35** 172–6
Mason J L and Mackay N A M 1976 Pain sensations associated with electrocutaneous stimulation *IEEE Trans. Biomed. Eng.* **23** 405–9
Medina L E and Grill W M 2014 Volume conductor model of transcutaneous electrical stimulation with kilohertz signals *J. Neural Eng.* **11** 066012
Merrill D R, Bikson M and Jefferys J G R 2005 Electrical stimulation of excitable tissue: design of efficacious and safe protocols *J. Neurosci. Methods* **141** 171–98
Minhas P, Bansal V, Patel J, Ho J S, Diaz J, Datta A and Bikson M 2010 Electrodes for high-definition transcutaneous DC stimulation for applications in drug-delivery and electrotherapy, including tDCS *J. Neurosci. Methods* **190** 188–97
Minhas P, Datta A and Bikson M 2011 Cutaneous perception during tDCS: role of electrode shape and sponge salinity *Clin. Neurophysiol.* **122** 637–8
Miranda P C, Lomarev M and Hallett M 2006 Modeling the current distribution during transcranial direct current stimulation *Clin. Neurophysiol.* **117** 1623–9
Mogensen M, Thrane L, Joergensen T M, Andersen P E and Jemec G B E 2009 Optical coherence tomography for imaging of skin and skin diseases *Semin. Cutan. Med. Surg.* **28** 196–202
Mueller E E, Loeffel R and Mead S 1953 Skin impedance in relation to pain threshold testing by electrical means *J. Appl. Physiol.* **5** 746–52
Nitsche M A *et al* 2008 Transcranial direct current stimulation: state of the art 2008 *Brain Stimul.* **1** 206–23
Olsen J, Themstrup L and Jemec G B E 2015 Optical coherence tomography in dermatology *G Ital. Dermatol. Venereol.* **150** 603–15
Opitz A, Paulus W, Will S, Antunes A and Thielscher A 2015 Determinants of the electric field during transcranial direct current stimulation *NeuroImage* **109** 140–50
Paneri B, Adair D, Thomas C, Khadka N, Patel V, Tyler W J, Parra L and Bikson M 2016 Tolerability of repeated application of transcranial electrical stimulation with limited outputs to healthy subjects *Brain Stimul.* **9** 740–54
Panescu D, Cohen K P, Webster J G and Stratbucker R A 1993 The mosaic electrical characteristics of the skin *IEEE Trans. Biomed. Eng.* **40** 434–9
Panescu D, Webster J G and Stratbucker R A 1994a A nonlinear finite element model of the electrode-electrolyte-skin system *IEEE Trans. Biomed. Eng.* **41** 681–7
Panescu D, Webster J G and Stratbucker R A 1994b A nonlinear electrical-thermal model of the skin *IEEE Trans. Biomed. Eng.* **41** 672–80
Pavšelj N, Préat V and Miklavčič D 2007 A numerical model of skin in vivo experiments *Ann. Biomed. Eng.* **35** 2138–44
Pierard-Franchimont C and Pierard G 2015 Sweat gland awakening on physical training: a skin capacitance mapping observation *Clin. Res. Dermatology* Open Access **2** 1–4
Poreisz C, Boros K, Antal A and Paulus W 2007 Safety aspects of transcranial direct current stimulation concerning healthy subjects and patients *Brain Res. Bull.* **72** 208–14
Reckow J, Rahman-Filipiak A, Garcia S, Schlaefflin S, Calhoun O, Dasilva A F, Bikson M and Hampstead B M 2018 Tolerability and blinding of 4 × 1 high-definition transcranial direct current stimulation (HD-tDCS) at two and three milliamps *Brain Stimul.* **11** 991–7
Sathi K A and Hosain M K 2020 Modeling and simulation of deep brain stimulation electrodes with various active contacts *Res. Biomed. Eng.* **36** 147–61
Saturnino G B, Antunes A and Thielscher A 2015 On the importance of electrode parameters for shaping electric field patterns generated by tDCS *NeuroImage* **120** 25–35
Saturnino G B, Thielscher A, Madsen K H, Knösche T R and Weise K 2019 A principled approach to conductivity uncertainty analysis in electric field calculations *Neuroimage* **188** 821–34
Schwan H P 1966 Alternating current electrode polarization *Biophysik* **3** 181–201
Sha N, Kenney L P J, Heller B W, Barker A T, Howard D and Moatamedi M 2008 A finite element model to identify electrode influence on current distribution in the skin *Artif. Organs* **32** 639–43
Shaw M T, Kasschau M, Dobbs B, Pawlak N, Pau W, Sherman K, Bikson M, Datta A and Charvet L E 2017 Remotely supervised transcranial direct current stimulation: an update on safety and tolerability *J. Vis. Exp.* **128** 1–8

Shiozawa P, da Silva M E, Raza R, Uchida R R, Cordeiro Q, Fregni F and Brunoni A R 2013 Safety of repeated transcranial direct current stimulation in impaired skin: a case report *J. Ect* **29** 147–8
Suchi T 1955 Experiments on electrical resistance of the human epidermis *Japan J. Physiol.* **5** 75–80
Torvi D A and Dale J D 1994 A finite element model of skin subjected to a flash fire *J. Biomech. Eng.* **116** 250–5
Tregear R T 1965 Interpretation of skin impedance measurements *Nature* **205** 600–1
Tregear R T 1966 *Physical Functions of Skin* (New York: Academic)
Truong D Q, Magerowski G, Blackburn G L, Bikson M and Alonso-Alonso M 2013 Computational modeling of transcranial direct current stimulation (tDCS) in obesity: impact of head fat and dose guidelines *Neuroimage Clin.* **2** 759–66
Turi Z *et al* 2019 Blinding is compromised for transcranial direct current stimulation at 1 mA for 20 min in young healthy adults *Eur. J. Neurosci.* **50** 3261–8
Wagner T, Fregni F, Fecteau S, Grodzinsky A, Zahn M and Pascual-Leone A 2007 Transcranial direct current stimulation: a computer-based human model study *NeuroImage* **35** 1113–24
Wake K, Sasaki K and Watanabe S 2016 Conductivities of epidermis, dermis, and subcutaneous tissue at intermediate frequencies *Phys. Med. Biol.* **61** 4376–89
Wallace D, Cooper N R, Paulmann S, Fitzgerald P B and Russo R 2016 Perceived comfort and blinding efficacy in randomised sham-controlled transcranial direct current stimulation (tDCS) trials at 2 mA in young and older healthy adults *PloS One* **11** e0149703
Wang B, Petrossians A and Weiland J D 2014 Reduction of edge effect on disk electrodes by optimized current waveform *IEEE Trans. Biomed. Eng.* **61** 2254–63
Wang J, Wei Y, Wen J and Li X 2015 Skin burn after single session of transcranial direct current stimulation (tDCS) *Brain Stimul.* **8** 165–6
Wei X F and Grill W M 2005 Current density distributions, field distributions and impedance analysis of segmented deep brain stimulation electrodes *J. Neural Eng.* **2** 139–47
Welzel J 2001 Optical coherence tomography in dermatology: a review *Skin Res. Technol.* **7** 1–9
Werner J and Buse M 1988 Temperature profiles with respect to inhomogeneity and geometry of the human body *J. Appl. Physiol.* **65** 1110–8
Wilson S B and Spence V A 1988 A tissue heat transfer model for relating dynamic skin temperature changes to physiological parameters *Phys. Med. Biol.* **33** 895–912
Woo E J, Hua P, Webster J G, Tompkins W J and Pallás-Areny R 1992 Skin impedance measurements using simple and compound electrodes *Med. Biol. Eng. Comput.* **30** 97–102
Woods A J *et al* 2016 A technical guide to tDCS, and related non-invasive brain stimulation tools *Clin. Neurophysiol.* **127** 1031–48
Workman C D, Fietsam A C and Rudroff T 2020 Transcranial direct current stimulation at 4 mA induces greater leg muscle fatigability in women compared to men *Brain Sci.* **10** 244
Yamamoto T and Yamamoto Y 1976 Electrical properties of the epidermal stratum corneum *Med. Biol. Eng.* **14** 151–8
Yamamoto T and Yamamoto Y 1977 Analysis for the change of skin impedance *Med. Biol. Eng. Comput.* **15** 219–27
Yousef H, Alhajj M and Sharma S 2020 Anatomy, skin (integument), epidermis *StatPearls* (Treasure Island, FL: StatPearls Publishing) (https://www.ncbi.nlm.nih.gov/books/NBK470464/)